The 2010 IEEE/RSJ International Conference on
Intelligent Robots and Systems
October 18-22, 2010, Taipei, Taiwan

Integrating IMU and Landmark Sensors for 3D SLAM and The Observability Analysis

Farhad Aghili

Abstract— **This paper investigates 3-dimensional Simultaneous Localization and Mapping (SLAM) and the corresponding observability analysis by fusing data from landmark sensors and a strap-down Inertial Measurement Unit (IMU) in an adaptive Kalman filter (KF). In addition to the vehicle's states and landmark positions, the self-tuning filter estimates the IMU calibration parameters as well as the covariance of the measurement noise. Examining the observability of the 3D SLAM system leads to the the conclusion that the system remains observable provided that at least one of these conditions is satisfied i) two known landmarks of which the connecting line is not collinear with the vector of the acceleration are observed ii) three known landmarks which are not placed in a straight line are observed.**

I. Introduction

To measure the pose of a vehicle with high bandwidth and long-term accuracy and stability usually involves data fusion of different sensors because there is no single sensor to satisfy both requirements. Inertial navigation systems where rate gyros and accelerations are integrated provides a high bandwidth pose measurement. However, long-term stability cannot be maintained because the integration inevitably results in quick accumulation of the position and attitude errors. Therefore, inertial systems require additional information about absolute position and orientation to overcome long-term drift [1].

Vision system and IMU are considered complementary positioning systems. Although vision systems provide low update rate, they are with the advantage of long-term position accuracy. Hence, fusion of vision and inertial navigation data, which are, respectively, accurate at low and high frequencies makes sense. Additionally, integration of the inertial data continuously provides pose estimation even when no landmark is observable or the vision is blocked for a short time. Most vision-based navigation systems work based on detecting several landmarks along which the vehicle pose is estimated. The challenge for localization of a vehicle traversing an unstructured environment is that the map of landmarks is not a priori known. The SLAM is referred to the capability to construct a map progressively in unknown environment being traversed by a vehicle and, at the same time, to estimate the vehicle pose using the map. In the past two decades, there have been great advancements in solving the SLAM problem together with compelling implementation of SLAM methods for field robotics [2]–[5]. Among other methods, the extended KF based SLAM has gained widespread acceptance in the robotic community [5], [6]. Observability analysis of the for 2-dimensional SLAM problem has been studied in the literature [7]–[10]. 3D SLAM and its implementation for mobile robots and airborne applications have been been proposed [11]–[16]. The observability of 3D SLAM has been also investigated in [16], [17]. However, 3D SLAM by integrating landmark sensors and IMU and the observability analysis of such a system is not addressed in these references.

This work is aimed at investigating at 3D Simultaneous Localization and Mapping and its corresponding observability analysis by fusing data from a 3D Camera and strap-down IMU in an adaptive KF. Since no wheel odometry is used in this methodology, it is applicable to terrestrial and aerial vehicles alike. The IMU calibration parameters in addition to the covariance matrix of the noise associated with the measurement landmarks' relative positions are estimated so that the KF filter is continually "tuned" as well as possible. The observability of such a technique for 3D SLAM is investigated and the observability conditions base on the number of fixed landmarks are derived.

II. Mathematical Model

A. Observation

Fig.1 illustrates the coordinate frames which are used to express the locations of a vehicle and landmarks. Coordinate frame $\{\mathcal{B}\}$ is attached to the vehicle, while $\{\mathcal{A}\}$ is the inertial frame. We assume that coordinate frames $\{\mathcal{B}\}$ and $\{\mathcal{A}\}$ are coincident at $t = 0$. Moreover, without loss of generality, we assume that $\{\mathcal{B}\}$ represents the frame of resolution of a landmark sensor as well as the IMU coordinate frame. The attitude of a rigid body relative to the specified inertial frame can be represented by a quaternion $\boldsymbol{q}^T = [\boldsymbol{q}_v^T \;\; q_o]$, where subscripts $_v$ and $_o$ denote the vector and scalar parts of the quaternion.

By definition, $\boldsymbol{q}_v = \boldsymbol{e} \sin\frac{\vartheta}{2}$ and $q_o = \cos\frac{\vartheta}{2}$, where $\boldsymbol{e}$ is a unit vector, known as the Euler axis, and ϑ is a rotation angle about this axis. Below, we review some basic definitions and properties of quaternions used in the rest of the paper. Consider quaternions $\boldsymbol{q}_1$, $\boldsymbol{q}_2$, and $\boldsymbol{q}_3$ and their corresponding rotation matrices $\boldsymbol{A}_1$, $\boldsymbol{A}_2$, and $\boldsymbol{A}_3$. Then,

$$\boldsymbol{A}_3 = \boldsymbol{A}_1\boldsymbol{A}_2 \quad \Longleftrightarrow \quad \boldsymbol{q}_3 = \boldsymbol{q}_2 \otimes \boldsymbol{q}_1$$

where $\boldsymbol{q}_3$ is obtained from the quaternion product. The quaternion product $[\boldsymbol{q}\otimes]$ is defined, analogous to the cross-product matrix, as

$$[\boldsymbol{q}\otimes] = \begin{bmatrix} q_o\mathbf{1}_3 - [\boldsymbol{q}_v\times] & \boldsymbol{q}_v \\ -\boldsymbol{q}_v^T & q_o \end{bmatrix}.$$

F. Aghili is a senior research scientist with Canadian Space Agency, Saint-Hubert, Quebec J3Y 8Y9, Canada, farhad.aghili@asc-csa.gc.ca

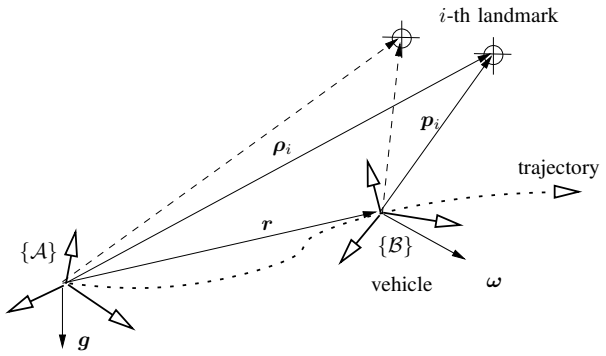

Fig. 1. Coordinate frames for 3D localization of a vehicle.

Also, the conjugate[1] $\boldsymbol{q}^*$ of a quaternion is defined such that $\boldsymbol{q}^* \otimes \boldsymbol{q} = \boldsymbol{q} \otimes \boldsymbol{q}^* = [0\ 0\ 0\ 1]^T$.

Let us assume that there exists a set of $n > 2$ landmarks which have a fixed position in the inertial frame, i.e.,

$$\dot{\boldsymbol{\rho}}_i = \mathbf{0}_{3\times 1} \qquad \forall i = 1, \cdots, n \tag{1}$$

The position of the landmarks in the vehicle frames, $\{\mathcal{B}\}$, are denoted by vectors $\boldsymbol{p}_1, \cdots \boldsymbol{p}_n$. The position and orientation of the vehicle with respect to the inertial frame are represented by vector $\boldsymbol{r}$ and unit quaternion $\boldsymbol{q}$, respectively. Apparently, from Fig. 1, we have

$$\boldsymbol{p}_i = \boldsymbol{A}^T(\boldsymbol{q})\big(\boldsymbol{\rho}_i - \boldsymbol{r}\big), \qquad \forall i = 1, \cdots, n. \tag{2}$$

where $\boldsymbol{A}(\boldsymbol{q})$ is the rotation matrix of frame $\{\mathcal{B}\}$ with respect to frame $\{\mathcal{A}\}$ that is related to the corresponding quaternion by

$$\boldsymbol{A}(\boldsymbol{q}) = (2q_o^2 - 1)\mathbf{1}_3 + 2q_o[\boldsymbol{q}_v\times] + 2\boldsymbol{q}_v\boldsymbol{q}_v^T. \tag{3}$$

The IMU is equipped with an accelerometer, which can be used for the measurements of vehicle acceleration. The acceleration equation can be written as

$$\boldsymbol{a} = \boldsymbol{A}^T(\boldsymbol{q})\big(\boldsymbol{g} + \ddot{\boldsymbol{r}}\big) - \boldsymbol{b}_a + \boldsymbol{v}_a, \tag{4}$$

where $\boldsymbol{a}$ is the accelerometer output, $\boldsymbol{g}$ is the gravity vector in frame $\{\mathcal{A}\}$; and $\boldsymbol{b}_a$ and $\boldsymbol{v}_a$ are the accelerometer bias and noise, respectively. We treat $\boldsymbol{v}_a$ as a random walk noise with covariance $E[\boldsymbol{v}_a\boldsymbol{v}_a^T] = \sigma_a^2\mathbf{1}_3$.

As suggested in [8], we assume that the map is anchored to a set of m landmarks observed at time $t = 0$. Without loss of generality, we can say that the initial pose is given by $\boldsymbol{r}(0) = \mathbf{0}_{3\times 1}$ and $\boldsymbol{A}(0) = \mathbf{1}_3$. Thus

$$\boldsymbol{\rho}_j = \boldsymbol{p}_j(0) \qquad \forall j = 1, \cdots, m.$$

The measurement vector includes the outputs of the accelerometer and the landmark sensor, i.e.,

$$\boldsymbol{z} = \begin{bmatrix}\boldsymbol{a}\\ \boldsymbol{p}\end{bmatrix} + \begin{bmatrix}\boldsymbol{v}_a\\ \boldsymbol{v}_p\end{bmatrix}, \tag{5}$$

where $\boldsymbol{p} = [\boldsymbol{p}_1^T, \cdots, \boldsymbol{p}_n^T]^T$, and vector $\boldsymbol{v}_p = [\boldsymbol{v}_{p_1}^T \cdots \boldsymbol{v}_{p_n}^T]^T$ is landmark sensor noise. Assuming that the noises of the landmark sensor and IMU are not mutually correlated, the covariance matrix of the measurement noise is given by

$$\boldsymbol{R} = E[\boldsymbol{v}\boldsymbol{v}^T] = \mathrm{diag}\{\sigma_a^2\mathbf{1}_3, \boldsymbol{R}_p\}, \tag{6}$$

where $\boldsymbol{R}_p$ is the covariance matrix of the landmark measurement noises. As will be later discussed in Section IV-D, factory-supplied value can be used for σ_a, while Kalman filter tries to estimate the remaining covariance.

Substituting (2) and (4) into (5) yields

$$\boldsymbol{z} = \boldsymbol{h} + \boldsymbol{v}, \tag{7a}$$

where

$$\boldsymbol{h} = \begin{bmatrix}\boldsymbol{A}^T(\boldsymbol{q})\big(\boldsymbol{g} + \ddot{\boldsymbol{r}}\big) - \boldsymbol{b}_a\\ \boldsymbol{A}^T(\boldsymbol{q})\big(\boldsymbol{\rho}_1 - \boldsymbol{r}\big)\\ \vdots\\ \boldsymbol{A}^T(\boldsymbol{q})\big(\boldsymbol{\rho}_n - \boldsymbol{r}\big)\end{bmatrix}. \tag{7b}$$

constitutes the nonlinear observation model. To linearize the observation vector, we need to derive the sensitivity of the nonlinear observation vector with respect to the system variables. Consider small orientation perturbations

$$\Delta\boldsymbol{q} = \boldsymbol{q} \otimes \bar{\boldsymbol{q}}^*. \tag{8}$$

around a nominal quaternion $\bar{\boldsymbol{q}}$—in the following, the bar sign stands for nominal value. Now, by virtue of $\boldsymbol{A}(\boldsymbol{q}) = \boldsymbol{A}(\Delta\boldsymbol{q} \otimes \bar{\boldsymbol{q}})$, one can compute the observation vector (7b) in terms of the perturbation $\Delta\boldsymbol{q}$. Using the first order approximation of nonlinear matrix function $\boldsymbol{A}^T(\Delta\boldsymbol{q})$ from expression (3) by assuming a small rotation $\Delta\boldsymbol{q}$, i.e., $\|\Delta\boldsymbol{q}_v\| \ll 1$ and $\Delta q_0 \approx 1$, we have

$$\boldsymbol{A}(\Delta\boldsymbol{q}) \approx \mathbf{1}_3 + 2[\Delta\boldsymbol{q}_v\times].$$

Therefore, by the first-order approximation, the observation vector can be written as as the following bilinear function

$$\boldsymbol{h} = \begin{bmatrix}\big(\mathbf{1}_3 - 2[\Delta\boldsymbol{q}_v\times]\big)\bar{\boldsymbol{A}}^T\big(\boldsymbol{g} + \ddot{\boldsymbol{r}}\big) - \boldsymbol{b}_a\\ \big(\mathbf{1}_3 - 2[\Delta\boldsymbol{q}_v\times]\big)\bar{\boldsymbol{A}}^T\big(\boldsymbol{\rho}_1 - \boldsymbol{r}\big)\\ \vdots\\ \big(\mathbf{1}_3 - 2[\Delta\boldsymbol{q}_v\times]\big)\bar{\boldsymbol{A}}^T\big(\boldsymbol{\rho}_n - \boldsymbol{r}\big)\end{bmatrix} + \text{HOT}.$$

Since out of the set of n landmarks there are m known landmarks, the entire state vector to be estimated is:

$$\boldsymbol{x} = [\boldsymbol{q}_v^T\ \boldsymbol{b}_g^T\ \boldsymbol{r}^T\ \dot{\boldsymbol{r}}^T\ \ddot{\boldsymbol{r}}^T\ \boldsymbol{b}_a^T\ \boldsymbol{\rho}_{m+1}^T\ \cdots\ \boldsymbol{\rho}_n^T]^T \in \mathbb{R}^{18+3(n-m)}, \tag{9}$$

where $\boldsymbol{b}_g$ is the gyro bias as will be later discussed in the next section. Thus, the observation sensitivity matrix $\boldsymbol{H} = \frac{\partial\boldsymbol{h}}{\partial\boldsymbol{x}}\big|_{\boldsymbol{A}=\bar{\boldsymbol{A}}}$ can be written as

$$\boldsymbol{H} = \begin{bmatrix}
2[\boldsymbol{c}\times] & \mathbf{0}_3 & \mathbf{0}_3 & \mathbf{0}_3 & \bar{\boldsymbol{A}}^T & -\mathbf{1}_3 & \mathbf{0}_3 & \cdots & \mathbf{0}_3\\
2[\boldsymbol{d}_1\times] & \mathbf{0}_3 & -\bar{\boldsymbol{A}}^T & \mathbf{0}_3 & \mathbf{0}_3 & \mathbf{0}_3 & \mathbf{0}_3 & \cdots & \mathbf{0}_3\\
\vdots & \vdots & \vdots & \vdots & \vdots & \vdots & \vdots & \vdots & \vdots\\
2[\boldsymbol{d}_m\times] & \mathbf{0}_3 & -\bar{\boldsymbol{A}}^T & \mathbf{0}_3 & \mathbf{0}_3 & \mathbf{0}_3 & \mathbf{0}_3 & \cdots & \mathbf{0}_3\\
2[\boldsymbol{d}_{m+1}\times] & \mathbf{0}_3 & -\bar{\boldsymbol{A}}^T & \mathbf{0}_3 & \mathbf{0}_3 & \mathbf{0}_3 & \bar{\boldsymbol{A}}^T & \cdots & \mathbf{0}_3\\
\vdots & \vdots & \vdots & \vdots & \vdots & \vdots & \vdots & \ddots & \vdots\\
2[\boldsymbol{d}_n\times] & \mathbf{0}_3 & -\bar{\boldsymbol{A}}^T & \mathbf{0}_3 & \mathbf{0}_3 & \mathbf{0}_3 & \mathbf{0}_3 & \cdots & \bar{\boldsymbol{A}}^T
\end{bmatrix}, \tag{10}$$

where $\boldsymbol{c} \triangleq \bar{\boldsymbol{A}}^T\big(\boldsymbol{g} + \ddot{\boldsymbol{r}}\big)$ and $\boldsymbol{d}_i \triangleq \bar{\boldsymbol{A}}^T(\boldsymbol{\rho}_i - \boldsymbol{r})$ for $i = 1, \cdots, n$.

[1] $q_o^* = q_o$ and $\boldsymbol{q}_v^* = -\boldsymbol{q}_v$.

B. Motion Dynamics

Denoting the angular velocity of the vehicle by $\boldsymbol{\omega}$, the relation between the time derivative of the quaternion and the angular velocity can be readily expressed by

$$\dot{\boldsymbol{q}} = \frac{1}{2}\underline{\boldsymbol{\omega}} \otimes \boldsymbol{q} \quad \text{where} \quad \underline{\boldsymbol{\omega}} = \begin{bmatrix} \boldsymbol{\omega} \\ 0 \end{bmatrix} \tag{11}$$

The angular rate obtained from the gyro measurement is

$$\boldsymbol{\omega}_g = \boldsymbol{\omega} - \boldsymbol{b}_g - \boldsymbol{\epsilon}_g \tag{12}$$

where $\boldsymbol{b}_g$ is the corresponding bias vector and $\boldsymbol{\epsilon}_g$ is the angular random walk noises with covariances $E[\boldsymbol{\epsilon}_g \boldsymbol{\epsilon}_g^T] = \sigma_g^2 \mathbf{1}_3$. The gyro bias is modeled as

$$\dot{\boldsymbol{b}}_g = \boldsymbol{\epsilon}_{b_g}, \tag{13}$$

where $\boldsymbol{\epsilon}_{b_g}$ is the random walk with covariances $E[\boldsymbol{\epsilon}_{b_g} \boldsymbol{\epsilon}_{b_g}^T] = \sigma_{b_g}^2 \mathbf{1}_3$. Adopting a linearization technique similar to [18], [19] one can linearize (11) about the nominal quaternion $\bar{\boldsymbol{q}}$ and nominal velocity

$$\bar{\boldsymbol{\omega}} = \boldsymbol{\omega}_g + \bar{\boldsymbol{b}}_g,$$

to obtain

$$\frac{\mathrm{d}}{\mathrm{d}t}\Delta\boldsymbol{q}_v = -\bar{\boldsymbol{\omega}} \times \Delta\boldsymbol{q}_v + \frac{1}{2}\Delta\boldsymbol{b}_g + \frac{1}{2}\boldsymbol{\epsilon}_g. \tag{14}$$

The process noise dynamics associated with the translational motion is considered as

$$\dddot{\boldsymbol{r}} = \boldsymbol{\epsilon}_w \quad \text{and} \quad \dot{\boldsymbol{b}}_a = \boldsymbol{\epsilon}_{b_a} \tag{15}$$

where $\boldsymbol{\epsilon}_w$ and $\boldsymbol{\epsilon}_{b_a}$ represent the process noise, which are assumed with covariances $E[\boldsymbol{\epsilon}_w \boldsymbol{\epsilon}_w^T] = \sigma_w^2 \mathbf{1}_3$ and $E[\boldsymbol{\epsilon}_{b_a} \boldsymbol{\epsilon}_{b_a}^T] = \sigma_{b_a}^2 \mathbf{1}_3$. Then, setting the dynamics equations (1), (13), (14), and (15) in the standard state space form, we get

$$\frac{\mathrm{d}}{\mathrm{d}t}\delta\boldsymbol{x} = \boldsymbol{F}\delta\boldsymbol{x} + \boldsymbol{G}\boldsymbol{\epsilon}, \tag{16a}$$

where $\boldsymbol{F} = \mathrm{diag}\{\boldsymbol{F}', \mathbf{0}_{(3n-6)\times(3n-6)}\}$,

$$\boldsymbol{F}' = \begin{bmatrix} -[\bar{\boldsymbol{\omega}}\times] & \frac{1}{2}\mathbf{1}_3 & \mathbf{0}_3 & \mathbf{0}_3 & \mathbf{0}_3 & \mathbf{0}_3 \\ \mathbf{0}_3 & \mathbf{0}_3 & \mathbf{0}_3 & \mathbf{0}_3 & \mathbf{0}_3 & \mathbf{0}_3 \\ \mathbf{0}_3 & \mathbf{0}_3 & \mathbf{0}_3 & \mathbf{1}_3 & \mathbf{0}_3 & \mathbf{0}_3 \\ \mathbf{0}_3 & \mathbf{0}_3 & \mathbf{0}_3 & \mathbf{0}_3 & \mathbf{1}_3 & \mathbf{0}_3 \\ \mathbf{0}_3 & \mathbf{0}_3 & \mathbf{0}_3 & \mathbf{0}_3 & \mathbf{0}_3 & \mathbf{0}_3 \\ \mathbf{0}_3 & \mathbf{0}_3 & \mathbf{0}_3 & \mathbf{0}_3 & \mathbf{0}_3 & \mathbf{0}_3 \end{bmatrix}, \tag{16b}$$

$$\boldsymbol{G} = \begin{bmatrix} \frac{1}{2}\mathbf{1}_3 & \mathbf{0}_3 & \mathbf{0}_3 & \mathbf{0}_3 \\ \mathbf{0}_3 & \mathbf{1}_3 & \mathbf{0}_3 & \mathbf{0}_3 \\ \mathbf{0}_3 & \mathbf{0}_3 & \mathbf{0}_3 & \mathbf{0}_3 \\ \mathbf{0}_3 & \mathbf{0}_3 & \mathbf{0}_3 & \mathbf{0}_3 \\ \mathbf{0}_3 & \mathbf{0}_3 & \mathbf{1}_3 & \mathbf{0}_3 \\ \mathbf{0}_3 & \mathbf{0}_3 & \mathbf{0}_3 & \mathbf{1}_3 \\ \multicolumn{4}{c}{\mathbf{0}_{(3n-6)\times 12}} \end{bmatrix}, \tag{16c}$$

and vector $\boldsymbol{\epsilon} = [\boldsymbol{\epsilon}_g^T \quad \boldsymbol{\epsilon}_{b_g}^T \quad \boldsymbol{\epsilon}_w^T \quad \boldsymbol{\epsilon}_{b_a}^T]^T$ contains the entire process noise.

III. Observability Analysis

A successful use of Kalman filtering requires that the system be observable. A linear time-invariant (LTI) systems is said to be *globally observable* if and only if its observability matrix is full rank. If a system is observable, the estimation error becomes only a function of the system noise, while the effect of the initial values of the states on the error will asymptotically vanish. The original observation model, (7), and a part of the process model, (11), are nonlinear systems. For nonlinear system, Hermann *et al.* proposed a rank condition test for "local weak observability" of nonlinear system that involves *Lie derivative* algebra [20]. Although this technique has been applied for observability of 2D SLAM [9], the analysis is too complex to be useful for the 3D case. The observability analysis can be simplified if the state-space is composed of the errors in terms of $\delta\boldsymbol{x}$. In that case, the time-varying system (10) and (16) can be replaced by a piecewise constant system for observability analysis [16], [21]. The intuitive motion is that such a time-varying system can be effectively approximated by a pieces-wise contact system without loosing the characteristic behavior of the original system [21].

Now assume that $\boldsymbol{F}_j$ be $\boldsymbol{H}_j$ are the jth time segment of the system's state transition matrix and observation model, respectively. Then, the observability matrix associated with linearized system (16) together with the observation model (10) is

$$\boldsymbol{\mathcal{O}}_j = \begin{bmatrix} \boldsymbol{H}_j^T & (\boldsymbol{H}_j\boldsymbol{F}_j)^T & \cdots & (\boldsymbol{H}_j\boldsymbol{F}_j^{3n+11})^T \end{bmatrix}^T.$$

The states of the system is instantaneously observable[2] if and only if

$$\text{rank } \boldsymbol{\mathcal{O}}_j = 3n + 12 \tag{17}$$

which is equivalent to $\boldsymbol{\mathcal{O}}_j$ having $3n + 12$ independent rows. In the following analysis, we remove the index $_j$ from the corresponding variables for the sake of simplicity of the notation. Now, we can construct the submatrices of the observability matrix as

$$\boldsymbol{HF} = \begin{bmatrix} -2[\boldsymbol{c}\times][\bar{\boldsymbol{\omega}}\times] & [\boldsymbol{c}\times] & \mathbf{0}_3 & \mathbf{0}_3 & \mathbf{0}_{3\times 3n} \\ -2[\boldsymbol{d}_1\times][\bar{\boldsymbol{\omega}}\times] & [\boldsymbol{d}_1\times] & \mathbf{0}_3 & -\bar{\boldsymbol{A}}^T & \mathbf{0}_{3\times 3n} \\ \vdots & \vdots & \vdots & \vdots & \vdots \\ -2[\boldsymbol{d}_n\times][\bar{\boldsymbol{\omega}}\times] & [\boldsymbol{d}_n\times] & \mathbf{0}_3 & -\bar{\boldsymbol{A}}^T & \mathbf{0}_{3\times 3n} \end{bmatrix} \tag{18a}$$

$$\boldsymbol{HF}^2 = \begin{bmatrix} 2[\boldsymbol{c}\times][\bar{\boldsymbol{\omega}}\times]^2 & -[\boldsymbol{c}\times][\bar{\boldsymbol{\omega}}\times] & \mathbf{0}_{3\times 6} & \mathbf{0}_3 & \mathbf{0}_{3\times(3n-3)} \\ 2[\boldsymbol{d}_1\times][\bar{\boldsymbol{\omega}}\times]^2 & -[\boldsymbol{d}_1\times][\bar{\boldsymbol{\omega}}\times] & \mathbf{0}_{3\times 6} & -\bar{\boldsymbol{A}}^T & \mathbf{0}_{3\times(3n-3)} \\ \vdots & \vdots & \vdots & \vdots & \vdots \\ 2[\boldsymbol{d}_n\times][\bar{\boldsymbol{\omega}}\times]^2 & -[\boldsymbol{d}_n\times][\bar{\boldsymbol{\omega}}\times] & \mathbf{0}_{3\times 6} & -\bar{\boldsymbol{A}}^T & \mathbf{0}_{3\times(3n-3)} \end{bmatrix} \tag{18b}$$

It is apparent from (10) that the sensitivity matrix $\boldsymbol{H}$ depends on the number of known or fixed landmarks, and hence so does the observability matrix. In the following analysis, we will derive the observability conditions for two cases: i) two known landmarks are observed, ii) three known landmarks are observed.

[2]Instantaneous observability means that the states over time period $[t_{j-1},\ t_j]$ can be estimated from the observation data over the same period [16].

A. Two Fixed Landmarks

We consider the observability of the SLAM when there are two fixed landmarks, i.e., $m = 2$. Before we pay our attention to the observability matrix, let us define

$$\boldsymbol{\Pi}_1 \triangleq [\boldsymbol{e}_1\times] + [\boldsymbol{c}\times] \tag{19}$$

where $\boldsymbol{e}_1 \triangleq \bar{\boldsymbol{A}}^T(\boldsymbol{\rho}_1 - \boldsymbol{\rho}_2)$. As shown in the Appendix, if matrix $\boldsymbol{\Pi}_1$ is invertible, then the following *block-triangular matrix* can be constructed from the observability matrix by few elementary Matrix Row Operations (MRO)

$$\boldsymbol{\mathcal{O}}_\Delta = \begin{bmatrix} 2\boldsymbol{\Pi}_1 & \mathbf{0}_3 & \mathbf{0}_3 & \mathbf{0}_3 & \mathbf{0}_3 & \mathbf{0}_3 & \mathbf{0}_3 & \cdots & \mathbf{0}_3 \\ \times & \boldsymbol{\Pi}_1 & \mathbf{0}_3 & \mathbf{0}_3 & \mathbf{0}_3 & \mathbf{0}_3 & \mathbf{0}_3 & \cdots & \mathbf{0}_3 \\ \times & \times & -\bar{\boldsymbol{A}}^T & \mathbf{0}_3 & \mathbf{0}_3 & \mathbf{0}_3 & \mathbf{0}_3 & \cdots & \mathbf{0}_3 \\ \times & \times & \times & -\bar{\boldsymbol{A}}^T & \mathbf{0}_3 & \mathbf{0}_3 & \mathbf{0}_3 & \cdots & \mathbf{0}_3 \\ \times & \times & \times & \times & -\bar{\boldsymbol{A}}^T & \mathbf{0}_3 & \mathbf{0}_3 & \cdots & \mathbf{0}_3 \\ \times & \times & \times & \times & \times & -\mathbf{1}_3 & \mathbf{0}_3 & \cdots & \mathbf{0}_3 \\ \times & \times & \times & \times & \times & \times & \bar{\boldsymbol{A}}^T & \cdots & \mathbf{0}_3 \\ & & & & & & & & \\ \times & \times & \times & \times & \times & \times & \times & \ddots & \mathbf{0}_3 \\ \times & \times & \times & \times & \times & \times & \times & \times & \bar{\boldsymbol{A}}^T \\ \vdots & \vdots & \vdots & \vdots & \vdots & \vdots & \vdots & \vdots & \vdots \end{bmatrix} \tag{20}$$

Note that rank$\boldsymbol{\mathcal{O}}$ = rank$\boldsymbol{\mathcal{O}}_\Delta$ because MRO preserves matrix rank. It is clear from (20) that the full rankness of the block-triangular matrix rests on the invertibility of the square matrix $\boldsymbol{\Pi}_1$. In other words, if $\boldsymbol{\Pi}_1$ is invertible, then the system is observable.

Proposition 1: If the line connecting two known landmarks, $\Delta\boldsymbol{\rho} = \boldsymbol{\rho}_1 - \boldsymbol{\rho}_2$, is not collinear with the vector of total acceleration $\boldsymbol{\alpha} = \boldsymbol{g} + \ddot{\boldsymbol{r}}$, then matrix $\boldsymbol{\Pi}_1$ is full-rank meaning that the observation matrix is full rank too.

PROOF: In a proof by contradiction, we show that $\boldsymbol{\Pi}_1 \in \mathbb{R}^{3\times3}$ must be a full-rank matrix if $\Delta\boldsymbol{\rho}$ and $\boldsymbol{\alpha}$ are not collinear. If $\boldsymbol{\Pi}_1$ is not full-rank, then there must exist a non-zero vector $\boldsymbol{\eta} \neq \mathbf{0}$ such that $\boldsymbol{\Pi}_1\boldsymbol{\eta} = \mathbf{0}$, i.e.,

$$\begin{aligned} & (\bar{\boldsymbol{A}}\Delta\boldsymbol{\rho}) \times \boldsymbol{\eta} + (\bar{\boldsymbol{A}}\boldsymbol{\alpha}) \times \boldsymbol{\eta} = \mathbf{0} \\ \Rightarrow \quad & \bar{\boldsymbol{A}}\big(\Delta\boldsymbol{\rho} \times (\bar{\boldsymbol{A}}^T\boldsymbol{\eta}) + \boldsymbol{\alpha} \times (\bar{\boldsymbol{A}}^T\boldsymbol{\eta})\big) = \mathbf{0} \\ \Rightarrow \quad & \Delta\boldsymbol{\rho} \times \boldsymbol{\eta}' + \boldsymbol{\alpha} \times \boldsymbol{\eta}' = \mathbf{0}, \end{aligned} \tag{21}$$

where $\boldsymbol{\eta}' = \bar{\boldsymbol{A}}^T\boldsymbol{\eta} \neq \mathbf{0}$. However, vectors $\Delta\boldsymbol{\rho} \times \boldsymbol{\eta}'$ and $\boldsymbol{\alpha} \times \boldsymbol{\eta}'$ can not annihilate one other because $\Delta\boldsymbol{\rho}$ and $\boldsymbol{\alpha}$ are not parallel. Thus, it is not possible for (21) to be true, meaning that matrix $\boldsymbol{\Pi}_1$ must be full rank and hence the system should be observable. □

B. Three Fixed Landmarks

Consider the case in which three known landmarks are observed, i.e., $m = 3$. Similar to (22), define the following matrix

$$\boldsymbol{\Pi}_2 \triangleq [\boldsymbol{e}_1\times] + [\boldsymbol{e}_2\times], \tag{22}$$

where $\boldsymbol{e}_2 \triangleq \bar{\boldsymbol{A}}^T(\boldsymbol{\rho}_3 - \boldsymbol{\rho}_1)$.

Remark 1: By using the same argument of Proposition 1, one can prove that matrix $\boldsymbol{\Pi}_2$ is full-rank if and only if vectors $\boldsymbol{e}_1$ and $\boldsymbol{e}_2$ are not collinear. In other words, if the three fixed landmarks are not located on a straight line, then matrix $\boldsymbol{\Pi}_2$ is full-rank.

Proposition 2: If the three known landmarks are not placed on a straight line, then the observation matrix is full rank.

PROOF: The observability matrix of the case of three fixed landmarks can be transformed to the following triangular matrix through almost similar MRO described in the Appendix

$$\boldsymbol{\mathcal{O}}_\Delta = \begin{bmatrix} 2\boldsymbol{\Pi}_2 & \mathbf{0}_3 & \mathbf{0}_3 & \mathbf{0}_3 & \mathbf{0}_3 & \mathbf{0}_3 & \mathbf{0}_3 & \cdots & \mathbf{0}_3 \\ \times & \boldsymbol{\Pi}_2 & \mathbf{0}_3 & \mathbf{0}_3 & \mathbf{0}_3 & \mathbf{0}_3 & \mathbf{0}_3 & \cdots & \mathbf{0}_3 \\ \times & \times & -\bar{\boldsymbol{A}}^T & \mathbf{0}_3 & \mathbf{0}_3 & \mathbf{0}_3 & \mathbf{0}_3 & \cdots & \mathbf{0}_3 \\ \times & \times & \times & -\bar{\boldsymbol{A}}^T & \mathbf{0}_3 & \mathbf{0}_3 & \mathbf{0}_3 & \cdots & \mathbf{0}_3 \\ \times & \times & \times & \times & -\bar{\boldsymbol{A}}^T & \mathbf{0}_3 & \mathbf{0}_3 & \cdots & \mathbf{0}_3 \\ \times & \times & \times & \times & \times & -\mathbf{1}_3 & \mathbf{0}_3 & \cdots & \mathbf{0}_3 \\ \times & \times & \times & \times & \times & \times & \bar{\boldsymbol{A}}^T & \cdots & \mathbf{0}_3 \\ & & & & & & & \ddots & \\ \times & \times & \times & \times & \times & \times & \times & \ddots & \mathbf{0}_3 \\ \times & \times & \times & \times & \times & \times & \times & \times & \bar{\boldsymbol{A}}^T \\ \vdots & \vdots & \vdots & \vdots & \vdots & \vdots & \vdots & \vdots & \vdots \end{bmatrix}. \tag{23}$$

Here, the first row of the above matrix is obtained by subtracting the fourth and third rows of matrix $\boldsymbol{H}$ from its second row and then adding the resultant row vectors. Performing the similar row operations on matrix $\boldsymbol{HF}$, (18a), yields the second row. The rest of rows are generated through the same elementary operations as described in the Appendix. In view of Remark 1, one can conclude that if the argument of Proposition 2 is held, then $\boldsymbol{\Pi}_2$ is full-rank and so is the observability matrix (23). □

C. Observability of Piecewise Constant Equivalent

Now assume that $\boldsymbol{H}_j$ and $\boldsymbol{F}_j$ vary from segment $j = 1$ to $j = r$. Then, the system (10)-(16) is to be completely observable if the *total observability matrix*

$$\tilde{\boldsymbol{\mathcal{O}}} = \begin{bmatrix} \boldsymbol{\mathcal{O}}_1 \\ \boldsymbol{\mathcal{O}}_1 e^{\boldsymbol{F}_1 t_{\Delta_1}} \\ \vdots \\ \boldsymbol{\mathcal{O}}_r e^{\boldsymbol{F}_{r-1} t_{\Delta_{r-1}}} \cdots e^{\boldsymbol{F}_1 t_{\Delta_1}} \end{bmatrix} \tag{24}$$

is full rank [21]. Moreover, if

$$\text{null}(\boldsymbol{\mathcal{O}}_j) \subset \text{null}(\boldsymbol{F}_j) \qquad \forall j = 1, \cdots, r \tag{25}$$

then it has been shown that null$(\tilde{\boldsymbol{\mathcal{O}}})$ = null$(\tilde{\boldsymbol{\mathcal{O}}}_s)$, where

$$\tilde{\boldsymbol{\mathcal{O}}}_s \triangleq [\boldsymbol{\mathcal{O}}_1^T \ \cdots \ \boldsymbol{\mathcal{O}}_r^T]^T \tag{26}$$

is the *stripped observability matrix* [21]. If the condition of the Propositions 1 or 2 for every single segment $j = 1, \cdots, r$ are satisfied, then the corresponding observability matrices are full rank, i.e., null$(\boldsymbol{\mathcal{O}}_j) = \emptyset$. Consequently, condition (25) in trivially satisfied and the stripped observability matrix (26) is full rank.

The above development in conjunction with Propositions 1 and 2 can be summarized in the following Remark:

Remark 2: Assume that linearized system (10)-(16) is piecewise constant for every single segment $j = 1, \cdots, r$. Then, the system during the time interval $t_1 \leq t \leq t_r$ is completely observable if at least one the following condition is satisfied

i) two known landmarks of which the connecting line is not collinear with the vector of the acceleration are observed
ii) three known landmarks which are not placed in a straight line are observed

IV. Estimator Design

A. Discrete-time Model

The equivalent discrete-time model of (16) is

$$\delta \boldsymbol{x}_{k+1} = \boldsymbol{\Phi}_k \delta \boldsymbol{x}_k + \boldsymbol{w}_k \tag{27}$$

where $\boldsymbol{\Phi}_k = \boldsymbol{\Phi}(t_k + t_\Delta, t_k)$ is the state transition matrix over time interval t_Δ and $\boldsymbol{w}_k$ is the equivalent discrete-time process noise. The state transition matrix takes a block diagonal form as $\boldsymbol{\Phi} = \text{diag}\{\boldsymbol{\Phi}, \mathbf{1}_{3n-6}\}$, and matrix $\boldsymbol{\Phi}' = \text{diag}\{\boldsymbol{\Phi}_r, \boldsymbol{\Phi}_t\}$ contains the state-transition matrices associated with the rotational system, $\boldsymbol{\Phi}_r$ and the translational systems, $\boldsymbol{\Phi}_t$. Assume that the nominal value of the angular velocity is given by

$$\bar{\boldsymbol{\omega}}_k = \hat{\boldsymbol{b}}_{g_k} + \boldsymbol{\omega}_{g_k}, \tag{28}$$

where the hat sign stands for estimation value, and define $\varpi_k \triangleq \|\bar{\boldsymbol{\omega}}_k\|$. Then, the state transition matrix $\boldsymbol{\Phi}_{r_k}(\tau) = \boldsymbol{\Phi}_r(\tau, t_k + \tau)$ takes on the form:

$$\boldsymbol{\Phi}_r(\tau) = \begin{bmatrix} \boldsymbol{\Phi}_{r_{11}}(\tau) & \boldsymbol{\Phi}_{r_{12}}(\tau) \\ \mathbf{0}_3 & \mathbf{1}_3 \end{bmatrix} \qquad 0 \le \tau \le t_\Delta \tag{29a}$$

where

$$\boldsymbol{\Phi}_{r_{11}} = \mathbf{1}_3 - \frac{\sin \varpi_k \tau}{\varpi_k}[\bar{\boldsymbol{\omega}}_k \times] + \frac{1 - \cos \varpi_k \tau}{\varpi_k^2}[\bar{\boldsymbol{\omega}}_k \times]^2$$

$$\boldsymbol{\Phi}_{r_{12}} = \frac{1}{2}\big(\mathbf{1}_3 \tau + \frac{\cos \varpi_k \tau - 1}{\varpi_k^2}[\bar{\boldsymbol{\omega}}_k \times] + \frac{\varpi_k \tau - \sin \varpi_k \tau}{\varpi_k^3}[\bar{\boldsymbol{\omega}}_k \times]^2\big)$$

The state-transition matrix associated with the translational motion is given by

$$\boldsymbol{\Phi}_t = \begin{bmatrix} \mathbf{1}_3 & t_\Delta \mathbf{1}_3 & \frac{t_\Delta^2}{2}\mathbf{1}_3 & \mathbf{0}_3 \\ \mathbf{0}_3 & \mathbf{1}_3 & t_\Delta \mathbf{1}_3 & \mathbf{0}_3 \\ \mathbf{0}_3 & \mathbf{0}_3 & \mathbf{1}_3 & \mathbf{0}_3 \\ \mathbf{0}_3 & \mathbf{0}_3 & \mathbf{0}_3 & \mathbf{1}_3 \end{bmatrix}. \tag{30}$$

In setting the corresponding process noise covariance matrix, $\boldsymbol{Q}_k = E[\boldsymbol{w}_k \boldsymbol{w}_k^T]$, a continuous-time white-noise model is assumed as follows

$$E[\boldsymbol{\epsilon}_k \boldsymbol{\epsilon}_k^T] = \boldsymbol{\Sigma}_k = \text{diag}(\sigma_g^2 \mathbf{1}_3, \sigma_{b_g}^2 \mathbf{1}_3, \sigma_w^2 \mathbf{1}_3, \sigma_{b_a}^2 \mathbf{1}_3).$$

With this assumption, the following process noise covariance matrix can be derived from

$$\boldsymbol{Q}_k = \int_{t_k}^{t_k + t_\Delta} \boldsymbol{\Phi}(t) \boldsymbol{G} \boldsymbol{\Sigma}_k \boldsymbol{G}^T \boldsymbol{\Phi}^T(t) \mathrm{d}t, \tag{31}$$

which has the following structure: $\boldsymbol{Q}_k = \text{diag}\{\boldsymbol{Q}_k', \mathbf{0}_{(3n-6)\times(3n-6)}\}$, where

$$\boldsymbol{Q}_k' = \begin{bmatrix} \boldsymbol{Q}_{r_{11}} & \boldsymbol{Q}_{r_{12}} & \mathbf{0}_3 \\ \times & \sigma_{b_g}^2 t_\Delta \mathbf{1}_3 & \mathbf{0}_3 \\ \times & \times & \boldsymbol{Q}_t \end{bmatrix}, \tag{32}$$

$$\boldsymbol{Q}_{r_{11}} = \big(\frac{\sigma_g^2 t_\Delta}{4} + \frac{\sigma_{b_g}^2 t_\Delta^2}{12}\big)\mathbf{1}_3 + \big(\frac{3\sigma_g^2 t_\Delta}{8\varpi_k^2} + \frac{\sigma_{b_g}^2 t_\Delta^3}{6\varpi_k^2} - \frac{3\sigma_{b_g}^2 t_\Delta}{8\varpi_k^4} + \frac{\sigma_g^2 \varpi_k^2 - \sigma_{b_g}^2}{16\varpi_k^5}\sin 2\varpi_k t_\Delta, + \frac{\sigma_{b_g}^2 t_\Delta}{2\varpi_k^4}\cos \varpi_k t_\Delta - \frac{\sigma_g^2}{2\varpi_k^3}\sin \varpi_k t_\Delta\big)[\bar{\boldsymbol{\omega}}_k \times]^2$$

$$\boldsymbol{Q}_{r_{12}} = \frac{\sigma_{b_g}^2 t_\Delta^2}{4}\mathbf{1}_3 + \frac{\sigma_{b_g}^2(\sin \varpi_k t_\Delta - \varpi_k t_\Delta)}{2\varpi_k^3}[\bar{\boldsymbol{\omega}}_k \times] + \frac{\sigma_{b_g}^2(2\cos \varpi_k t_\Delta + \varpi_k^2 t_\Delta^2 - 2)}{4\varpi_k^4}[\bar{\boldsymbol{\omega}}_k \times]^2,$$

$$\boldsymbol{Q}_t = \begin{bmatrix} \frac{\sigma_r^2}{20} t_\Delta^5 \mathbf{1}_3 & \frac{\sigma_w^2}{8} t_\Delta^4 \mathbf{1}_3 & \frac{\sigma_w^2}{6} t_\Delta^3 \mathbf{1}_3 & \mathbf{0}_3 \\ \times & \frac{\sigma_w^2}{3} t_\Delta^3 \mathbf{1}_3 & \frac{\sigma_w^2}{2} t_\Delta^2 \mathbf{1}_3 & \mathbf{0}_3 \\ \times & \times & \sigma_w^2 t_\Delta \mathbf{1}_3 & \mathbf{0}_3 \\ \times & \times & \times & \sigma_{b_a}^2 t_\Delta \mathbf{1}_3 \end{bmatrix}.$$

B. Extended Kalman Filter Cycle

Before we pay attention to the EKF estimator design, it is important to point out that only the variation of the quaternion, $\Delta \boldsymbol{q}_{v_k}$, and not the quaternion itself, $\boldsymbol{q}_k$, is estimated by the KF. Nevertheless, the full quaternion can be obtained from the former variables if the value of the nominal quaternion $\bar{\boldsymbol{q}}(t_k)$ is given, i.e.,

$$\Delta \hat{\boldsymbol{q}}_k^- = \hat{\boldsymbol{q}}_k^- \otimes \bar{\boldsymbol{q}}^*(t_k) \tag{34}$$

For the linearization of the quaternion to make sense, the nominal quaternion trajectory, $\bar{\boldsymbol{q}}(t)$, should be close to actual one as much as possible. A natural choice for *a posteriori* nominal value of quaternion at t_{k-1} is its update estimate, i.e., $\bar{\boldsymbol{q}}(t_{k-1}) = \hat{\boldsymbol{q}}_{k-1}$. Since the nominal angular velocity $\bar{\boldsymbol{\omega}}_k$ is assumed constant at interval $t_{k-1} \le t \le t_k$, then according to (11) the nominal quaternion evolves from its initial value $\bar{\boldsymbol{q}}(t_{k-1})$ to its *a priori* value $\bar{\boldsymbol{q}}(t_k)$ by

$$\bar{\boldsymbol{q}}_k \triangleq \bar{\boldsymbol{q}}(t_k) = e^{\frac{t_\Delta}{2}[\underline{\bar{\boldsymbol{\omega}}}_k \otimes]} \hat{\boldsymbol{q}}_{k-1}, \tag{35}$$

which will be used at the innovation step of KF. The above exponential matrix function has the following closed-form expression

$$e^{\frac{t_\Delta}{2}[\underline{\bar{\boldsymbol{\omega}}}_k \otimes]} = \big(\cos \frac{\varpi_k t_\Delta}{2} + \sin \frac{\varpi_k t_\Delta}{2}\big)\mathbf{1}_4 + \big(\frac{2}{\varpi_k t_\Delta}\sin \frac{\varpi_k t_\Delta}{2} - \frac{1}{2}\cos \frac{\varpi_k t_\Delta}{2}\big)[\underline{\bar{\boldsymbol{\omega}}}_k \otimes]$$

The EKF-based observer has two steps: (i) Estimate correction and (ii) estimation propagation. The estimate correction process begins by calculating the filter gain matrix as

$$\boldsymbol{K}_k = \boldsymbol{P}_k^- \boldsymbol{H}_k^T \big(\boldsymbol{H}_k \boldsymbol{P}_k^- \boldsymbol{H}_k^T + \boldsymbol{R}\big)^{-1} \tag{36a}$$

Next, the states of KF and the covariance matrix are updated in the innovation step. Recall that only the vector part of the quaternion variation, not the full quaternion, is included in the KF state vector. Therefore, we use a priori value of the nominal quaternion $\bar{\boldsymbol{q}}_k \triangleq \bar{\boldsymbol{q}}(t_k)$ from expression (35) first to calculate the *a priori* quaternion deviation and then, after the

state update in the innovation step, *a posteriori* quaternion deviation is recombined with the nominal quaternion to obtain the quaternion update. That is

$$\begin{bmatrix}\Delta\hat{\boldsymbol{q}}_{v_k}\\ \hat{\boldsymbol{y}}_k\end{bmatrix} = \begin{bmatrix}\mathrm{vec}(\hat{\boldsymbol{q}}_k^- \otimes \bar{\boldsymbol{q}}_k^*)\\ \hat{\boldsymbol{y}}_k^-\end{bmatrix} + \boldsymbol{K}_k\big(\boldsymbol{z}_k - \boldsymbol{h}_k(\hat{\boldsymbol{x}}_k^-)\big) \quad (36b)$$

$$\hat{\boldsymbol{q}}_k = \Delta\hat{\boldsymbol{q}}_k \otimes \bar{\boldsymbol{q}}_k = \begin{bmatrix}\Delta\hat{\boldsymbol{q}}_{v_k}\\ \sqrt{1-\|\Delta\hat{\boldsymbol{q}}_{v_k}\|^2}\end{bmatrix} e^{\frac{t_\Delta}{2}[\bar{\boldsymbol{\omega}}_k\otimes]}\hat{\boldsymbol{q}}_{k-1} \quad (36c)$$

Note that $\Delta\hat{\boldsymbol{q}}_{v_k}^- = \mathrm{vec}(\hat{\boldsymbol{q}}_k^- \otimes \bar{\boldsymbol{q}}_k^*)$ in (36b) is a priori estimation of the quaternion deviation, where $\mathrm{vec}(\cdot)$ returns the vector part of a quaternion. The covariance matrix is updated according to

$$\boldsymbol{P}_k = \big(\mathbf{1}_{3n+12} - \boldsymbol{K}_k\boldsymbol{H}_k\big)\boldsymbol{P}_k^-, \quad (36d)$$

In the second step, the states and the covariance matrix are propagated into the next time step. Combining equations of (1), (11), (13), and (15), we then get the state-space model of the system as

$$\dot{\boldsymbol{x}} = \boldsymbol{f}(\boldsymbol{x}, \boldsymbol{\epsilon}),$$

which can be used for estimating propagation of the states. Thus

$$\hat{\boldsymbol{x}}_{k+1}^- = \hat{\boldsymbol{x}}_k + \int_{t_k}^{t_k+t_\Delta} \boldsymbol{f}(\boldsymbol{x}(t), \mathbf{0})\,\mathrm{d}t \quad (37a)$$

$$\boldsymbol{P}_{k+1}^- = \boldsymbol{\Phi}_k\boldsymbol{P}_k\boldsymbol{\Phi}_k^T + \boldsymbol{Q}_k \quad (37b)$$
$$= \begin{bmatrix}\boldsymbol{\Phi}_k'\begin{bmatrix}\boldsymbol{P}_{11} & \boldsymbol{P}_{12}^T\\ \boldsymbol{P}_{12} & \boldsymbol{P}_{22}\end{bmatrix}\boldsymbol{\Phi}_k'^T + \boldsymbol{Q}_k' & \times\\ \boldsymbol{P}_{22}, & \end{bmatrix},$$

where $\boldsymbol{P}_{11} \in \mathbb{R}^{18\times 18}$ and the other submatrices are obtained from adequate partitioning of the covariance matrix.

C. Landmark Augmentation

The KF estimation proceeds according to (36)-(37) cycle as long as the landmarks are reobserved. However, if a new landmark is observed then the KF states and its covariance matrix have to be augmented. Let us assume $\boldsymbol{z}_{\mathrm{new}}$ represent the observation associated with a new landmark at location $\boldsymbol{\rho}_{\mathrm{new}}$. Then, the explicit expression of the new landmark position can be obtained from the inverse kinematics of the observation as

$$\begin{aligned}\boldsymbol{\rho}_{\mathrm{new}} &= \boldsymbol{A}(\Delta\boldsymbol{q}\otimes\bar{\boldsymbol{q}})(\boldsymbol{z}_{\mathrm{new}} - \boldsymbol{v}_{\mathrm{new}}) + \boldsymbol{r}\\ &\approx \bar{\boldsymbol{A}}(\mathbf{1}_3 + 2[\Delta\boldsymbol{q}_v\times])(\boldsymbol{z}_{\mathrm{new}} - \boldsymbol{v}_{\mathrm{new}}) + \boldsymbol{r}\\ &\approx \bar{\boldsymbol{A}}\boldsymbol{z}_{\mathrm{new}} + \hat{\boldsymbol{r}} \underbrace{-\bar{\boldsymbol{A}}\boldsymbol{v}_{\mathrm{new}} - 2\bar{\boldsymbol{A}}[\boldsymbol{z}_{\mathrm{new}}\times]\Delta\tilde{\boldsymbol{q}}_v + \tilde{\boldsymbol{r}}}_{\mathrm{noise}}\end{aligned}$$

where $\tilde{\boldsymbol{q}}_v$ and $\tilde{\boldsymbol{r}}$ are the corresponding estimation errors and $\boldsymbol{R}_{\mathrm{new}} = E[\boldsymbol{v}_{\mathrm{new}}\boldsymbol{v}_{\mathrm{new}}^T]$. Consequently, the states and covariance matrix are augmented as

$$\hat{\boldsymbol{x}}_{\mathrm{new}} = \begin{bmatrix}\hat{\boldsymbol{x}}\\ \bar{\boldsymbol{A}}\boldsymbol{z}_{\mathrm{new}} + \hat{\boldsymbol{r}}\end{bmatrix} \quad \text{and} \quad \boldsymbol{P}_{\mathrm{new}} = \begin{bmatrix}\boldsymbol{P} & \boldsymbol{\Upsilon}^T\\ \boldsymbol{\Upsilon} & \bar{\boldsymbol{A}}\boldsymbol{R}_{\mathrm{new}}\bar{\boldsymbol{A}}^T\end{bmatrix}$$

where

$$\boldsymbol{\Upsilon} = \begin{bmatrix}-2\bar{\boldsymbol{A}}[\boldsymbol{z}_{\mathrm{new}}\times] & \mathbf{0}_3 & \mathbf{1}_3 & \mathbf{0}_{3\times(3n+6)}\end{bmatrix}\boldsymbol{P}.$$

D. Noise-Adaptive Filter

Efficient implementation of the KF requires the statistical characteristics of the measurement noise (6). The IMU noises are not usually characterized by a time-invariant covariance. Therefore, σ_a can be treated as a constant parameter, which can be either derived from the sensor specification or empirically tuned. However, the landmark measurement errors may vary from one point to the next. Therefore, in order to improve the quality of the state estimate, it would be desirable to weight the landmark measurement with the "good" data more heavily than the one with "poor" data in the estimator. This requires readjusting the covariance matrix associated with $\boldsymbol{v}_p$ in the filter's internal model, so that the filter is continually "tuned" as well as possible based upon information obtained in real time from the measurements.

In a noise-adaptive Kalman filter, the issue is that, in addition to the states, the covariance matrix of the measurement noise has to be estimated. Let us define the residual error

$$\boldsymbol{\varrho}_k \triangleq \boldsymbol{p}_k - \boldsymbol{L}_k\hat{\boldsymbol{\chi}}_k^- \quad \text{where} \quad \boldsymbol{L}_k = \begin{bmatrix}2[\boldsymbol{d}_{1_k}\times] & \mathbf{1}_3\\ \vdots & \vdots\\ 2[\boldsymbol{d}_{n_k}\times] & \mathbf{1}_3\end{bmatrix},$$

$\boldsymbol{\chi}_k = [\Delta\boldsymbol{q}_{v_k}^T \;\; \boldsymbol{r}_k^T]^T$. Then the following identity holds

$$\boldsymbol{\varrho}_k = \boldsymbol{L}_k(\boldsymbol{\chi}_k - \hat{\boldsymbol{\chi}}_k^-) + \boldsymbol{v}_{p_k}.$$

Taking variance of both sides of the above equation gives

$$\boldsymbol{R}_{p_k} = \boldsymbol{W}_k - \boldsymbol{L}_k\boldsymbol{P}_{\chi_k}^-\boldsymbol{L}_k^T \quad \text{with} \quad \boldsymbol{W}_k = E[\boldsymbol{\varrho}_k\boldsymbol{\varrho}_k^T].$$

Note that the covariance matrix $\boldsymbol{P}_{\chi_k}^- = E[\tilde{\boldsymbol{\chi}}_k\tilde{\boldsymbol{\chi}}_k^T]$, where $\tilde{\boldsymbol{\chi}}_k = \boldsymbol{\chi}_k - \hat{\boldsymbol{\chi}}_k^-$, can be extracted from the covariance matrix of the Kalman filter, $\boldsymbol{P}_k^-$. The above equation can be used to estimate the measurement covariance matrix $\hat{\boldsymbol{R}}_{p_k}$ from an an ergodic approximation of the covariance of the zero-mean residual $\boldsymbol{\varrho}$ in the sliding sampling window with finite length w. That is

$$\hat{\boldsymbol{W}}_k \approx \frac{1}{w}\sum_{i=k-w}^{k}\boldsymbol{\varrho}_i\boldsymbol{\varrho}_i^T \quad (38a)$$
$$= \hat{\boldsymbol{W}}_{k-1} + \frac{1}{w}\Big(\boldsymbol{\varrho}_k\boldsymbol{\varrho}_k^T - \boldsymbol{\varrho}_{k-w}\boldsymbol{\varrho}_{k-w}^T\Big). \quad (38b)$$

where w is chosen empirically to give some statistical smoothing, i.e., w should take a small value if the statistical characteristic of the landmark sensor noises change significantly over time, conversely, it takes a large w if the noise is stationary.

V. A Case Study

A series of case studies were conducted on the CSA's red-rover traversing the 30×60 m Mars Emulation Terrain (MET), as shown in Fig. 2, in order to demonstrate the convergence property of the 3D SLAM with respect to different numbers of fixed landmarks. The rover is equipped with IMU plus three RTK GPS antennas, which allows to measure not only the vehicle position but also its attitude using the method described in [22]. Consequently, the vehicle pose

Fig. 2. CSA Mars emulation terrain.

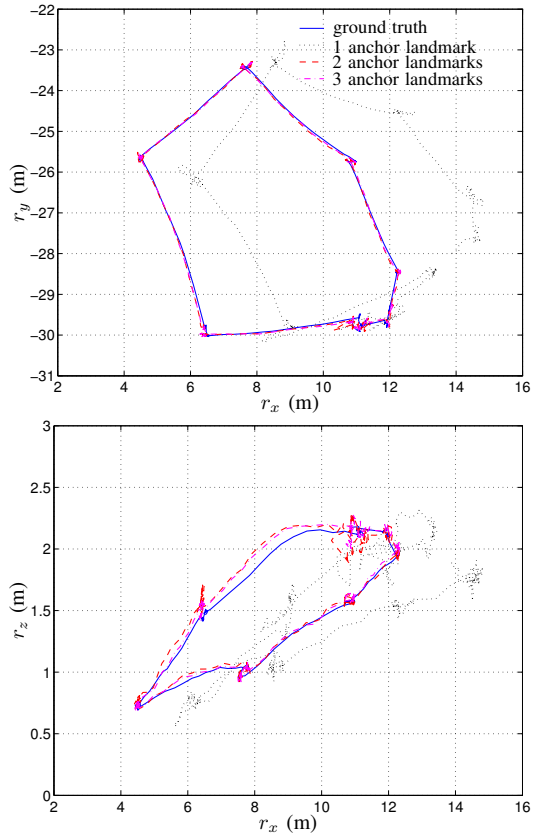

Fig. 3. 3D path taken by the vehicle.

trajectories obtained from the GPS system are considered as the "ground-truth" path.

Figs. 3 and 4A show the 3D path taken by the mobile robot and its attitude, respectively, while the vehicle passing through seven via points. The IMU measurements are received at the rate of 20 Hz, and the corresponding trajectories are depicted in Figs. 5. In this case study, the relative positions of the landmarks are simulated by using the ground truth trajectories and a set of random noise sequences with difference standard deviations bounded by $0.1 < \sigma_{p_i} < 0.25$ (m). The filter processed the data from three scenarios as: (i) one of the observed landmarks used as a global reference, (ii) two of the observed landmarks used

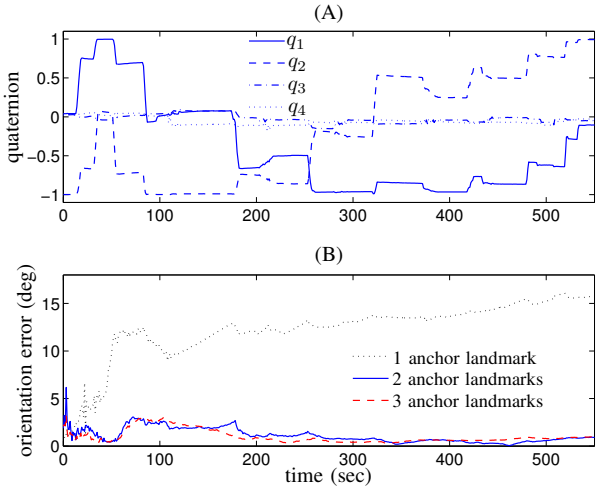

Fig. 4. Estimation of vehicle attitude.

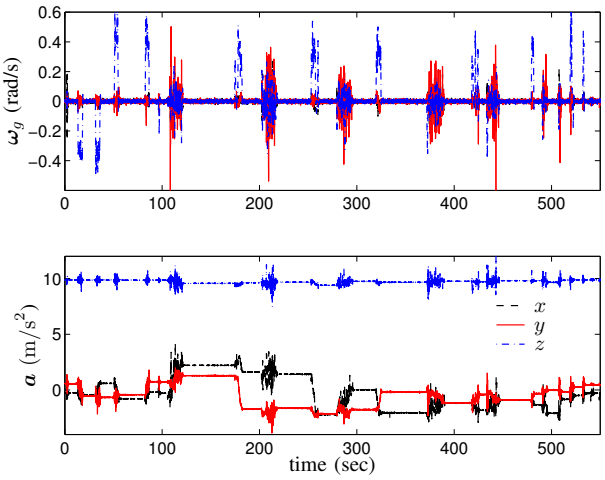

Fig. 5. IMU outputs.

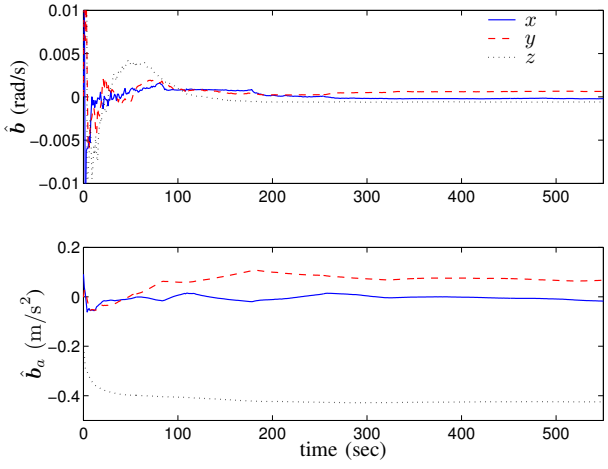

Fig. 6. Estimation of the IMU calibration parameters.

as a global reference (iii) three of the observed landmarks used as a global reference. Figs. 3 shows trajectories of the position estimates for the three cases, while the corresponding orientation estimate errors are shown in 4B. Here, the orientation errors is calculated by

$$\text{Orientation Error} = 2\sin^{-1}\|\text{vec}(\hat{\boldsymbol{q}}^* \otimes \boldsymbol{q}_{\text{ref}})\|. \qquad (39)$$

It is evident from the graphs that the filter did not converge if only one of the first observed landmark is used as the global reference. However, the results clearly show that the pose estimates very well converges to the actual values if either two or three of the observed landmarks are used as the global references. Fig. 6 illustrates the time history of the estimates of the gyroscope bias and the accelerometer bias.

VI. Conclusions

Development and the corresponding observability analysis of a 3D SLAM by fusing IMU and landmark sensors in an adaptive KF have been presented. Examining the observability of such SLAM technique in 3-dimensional environment led to the conclusion that the system is observable if at least one of the following condition is satisfied: i) two known landmarks of which the connecting line is not collinear with the vector of the acceleration are observed ii) three known landmarks which are not placed in a straight line are observed. The IMU calibration parameters and the covariance matrix of measurement noise associated with landmark sensors were estimated upon the sensor information obtained in real time so that the KF filter is continually "tuned" as well as possible.

Appendix

The following matrix,

$$\begin{bmatrix}
2\boldsymbol{\Pi}_1 & \mathbf{0}_3 & \mathbf{0}_3 & \mathbf{0}_3 & \bar{\boldsymbol{A}}^T & -\mathbf{1}_3 & \mathbf{0}_3 & \cdots & \mathbf{0}_3 \\
\times & \boldsymbol{\Pi}_1 & \mathbf{0}_3 & \mathbf{0}_3 & \mathbf{0}_3 & \mathbf{0}_3 & \mathbf{0}_3 & \cdots & \mathbf{0}_3 \\
\times & \times & -\bar{\boldsymbol{A}}^T & \mathbf{0}_3 & \mathbf{0}_3 & \mathbf{0}_3 & \mathbf{0}_3 & \cdots & \mathbf{0}_3 \\
\times & \times & \times & -\bar{\boldsymbol{A}}^T & \mathbf{0}_3 & \mathbf{0}_3 & \mathbf{0}_3 & \cdots & \mathbf{0}_3 \\
\times & \times & \times & \times & -\bar{\boldsymbol{A}}^T & \mathbf{0}_3 & \mathbf{0}_3 & \cdots & \mathbf{0}_3 \\
\times & \times & \times & \times & \times & -\mathbf{1}_3 & \mathbf{0}_3 & \cdots & \mathbf{0}_3 \\
\times & \times & \times & \times & \times & \times & \bar{\boldsymbol{A}}^T & \cdots & \mathbf{0}_3 \\
 & & & & & & & \ddots & \\
\times & \times & \times & \times & \times & \times & \times & \times & \mathbf{0}_3 \\
\times & \times & \times & \times & \times & \times & \times & \times & \bar{\boldsymbol{A}}^T
\end{bmatrix}, \qquad (40)$$

can be constructed via the following elementary operations: The first row of the above matrix is obtained by subtracting the third row from the second row of matrix $\boldsymbol{H}$, (10), and then adding the first row of matrix $\boldsymbol{H}$. Performing the similar row operations on matrix $\boldsymbol{HF}$, (18a), yields the second row of the above matrix. The third to sixth rows of matrix (40) are picked from the second rows of matrices $\boldsymbol{H}$, $\boldsymbol{HF}$, and $\boldsymbol{HF}^2$, (18b), plus the first row of matrix $\boldsymbol{H}$, respectively. Finally, the remaining rows of matrix (40) are picked from the fourth to n rows of matrix $\boldsymbol{H}$. Since $\boldsymbol{\Pi}$ and $\bar{\boldsymbol{A}}^T$ are invertible matrices, one can show that $\bar{\boldsymbol{A}}^T$ and $-\mathbf{1}_3$ terms appeared in the first row of the above matrix can be eliminated by adequate linear combinations of other row vectors.

References

[1] B. Barshan and H. F. Durrant-Whyte, "Inertial navigation systems for mobile robots," *IEEE Trans. on Robotics & Automation*, vol. 11, no. 3, pp. 328–342, June 1995.

[2] R. Smith, M. Self, and P. Cheesman, *Estimating Uncertain Spatial Relationship in Robotics, Autonomous Robot Vehicle*, I. Cox and G. Wilfong, Eds. New York: Springer-Verlag, 1987.

[3] H. F. Durant-Whyte, "Uncertain geometry in robotics," *IEEE Trans. on Robotics & Autimation*, vol. 4, no. 1, pp. 23–31, 1988.

[4] N. Ayache and O. Faugeras, "Maintaining a representation of the environment of a mobile robot," *IEEE Trans. on Robotics & Automation*, vol. 5, no. 6, pp. 804–819, 1998.

[5] J. J. Leonard and H. F. Durrant-Whyte, "Simultaneous map building and localization for an autonomous mobile robot," in *IEEE/RSJ Int. Workshop on Intelligent Robots and Systems*, Osaka, Japan, November 1991, pp. 1442–1447.

[6] B. Xi, R. Guo, F. Sun, and Y. Huang, "Simulation research for active simultaneous localization and mapping based on extended kalman filter," in *IEEE/RSJ Int. Conference on Intelligent Robots and Systems*, Qingdao, China, September 2008, pp. 2443–2448.

[7] Z. Chen, K. Jiang, and J. C. Hung, "Local observability matrix and its application to observability analysis," in *16th Annual Conference of IEEE (IECON'90)*, Pacific Grove, CA, USA, November 1990, pp. 100–103.

[8] J. Andrade-Cetto and A. Sanfeliu, "The effects of partial observability when building fully correlated maps," *IEEE Trans. on Robotics & Autimation*, vol. 21, no. 4, pp. 771–777, 2005.

[9] K. W. L. amd W. S. Wijesoma and J. I. Guzman, "On the observability and observability analysis of SLAM," in *IEEE/RSJ Int. Conference on Intelligent Robots and Systems*, Beijing, China, October 2006, pp. 3569–3574.

[10] S. Huang and G. Dissanayake, "Convergence analysis for extended kalman filter based SLAM," in *IEEE Int. Conf. on Robotics & Automation*, Orlando, Florida, May 2006, pp. 1556–1563.

[11] H. Surmann, A. Nuchter, K. Lingemann, and J. Hetzberg, "6D SLAM - preliminary report on closing the loop in six dimension," in *Proceedings of the 5th IFAC/EURON Symposium on Intelligent Autonomous Vehicles (IVA)*, Lisbon, Portugal, July 2004.

[12] J. Kim and A. Sukkarieh, "Autonomous airborne navigation in unknown terrain environment," *IEEE Trans. on Aerospace & Electronic Systems*, vol. 40, no. 3, pp. 1031–1045, July 2004.

[13] A. Nuechter, K. Lingemann, J. Hertzberg, and H. Surmann, "6D SLAM-mapping outdoor environment," in *IEEE Int. Workshop of Safety, Security and Rescue Robotics*, Gaithersburg, Maryland USA, August 2006.

[14] J. Kim and S. Sukkarieh, "Real-time implementation of airborne inertial-SLAM," *Robotics and Autonomous Systems*, vol. 55, no. 1, pp. 519–535, 2007.

[15] S. Abdallah, D. Asmar, and J. Zelek, "A benchmark for outdoor SLAM systems," *Journal of Field Robotics*, vol. 24, no. 1-2, pp. 145–165, 2007.

[16] M. Bryson and S. Sukkarieh, "Observability analysis and active control for airborne slam," *Aerospace and Electronic Systems, IEEE Transactions on*, vol. 44, no. 1, pp. 261 –280, january 2008.

[17] A. Nemra and N. Aouf, "Robust airborne 3d visual simultaneous localization and mapping with observability and consistency analysis," *Journal of Intelligent and Robotic Systems*, vol. 55, no. 4–5, pp. 345–376, 2009.

[18] E. J. Lefferts, F. L. Markley, and M. D. Shuster, "Kalman filtering for spacecraft attitude estimation," *Journal of Guidance*, vol. 5, no. 5, pp. 417–429, September–October 1982.

[19] M. E. Pittelkau, "Kalman filtering for spacecraft system alignment calibration," *Journal of Guidance, Control, and Dynamics*, vol. 24, no. 6, pp. 1187–1195, November 2001.

[20] R. Hermann and A. Krener, "Nonlinear controllability and observability," *Automatic Control, IEEE Transactions on*, vol. 22, no. 5, pp. 728 – 740, oct 1977.

[21] D. Goshen-Meskin and I. Y. Bar-Itzhack, "Observability analysis of piece-wise constant systems. i. theory," *Aerospace and Electronic Systems, IEEE Transactions on*, vol. 28, no. 4, pp. 1056 –1067, oct 1992.

[22] F. Aghili and A. Salerno, "Attitude determination and localization of mobile robots using two RTK GPSs and IMU," in *IEEE/RSJ International Conference on Intelligent Robots & Systems*, St. Louis, USA, October 2009, pp. 2045–2052.